Hierarchical Morphogenesis of Swallowtail Butterfly Wing Scale Nanostructures

Kwi Shan Seah[1,2] and Vinodkumar Saranathan*[1-5]

Affiliations:

[1]Division of Science, Yale-NUS College, 10 College Avenue West, 138609, Singapore.

[2]Department of Biological Science, National University of Singapore, 117543, Singapore.

[3]NUS Nanoscience and Nanotechnology Initiative (NUSNNI-NanoCore), National University of Singapore, 117581, Singapore.

[4]Lee Kong Chian Natural History Museum, National University of Singapore, 117377, Singapore.

[5]Present Address: Division of Sciences, School of Interwoven Arts and Sciences, Krea University, 5655, Central Expressway, Sri City, Andhra Pradesh 517646, India.

*E-mail : Vinodkumar.Saranathan@aya.yale.edu

Orcid IDs: KSS: 0000-0001-8451-3732; VS: 0000-0003-4058-5093

Abstract:

The study of color patterns in the animal integument is a fundamental question in biology, with many lepidopteran species being exemplary models in this endeavor due to their relative simplicity and elegance. While significant advances have been made in unravelling the cellular and molecular basis of lepidopteran pigmentary coloration, the morphogenesis of wing scale nanostructures involved in structural color production

is not well understood. Contemporary research in this topic largely focuses on a few nymphalid model taxa (*e.g.*, *Bicyclus*, *Heliconius*), despite an overwhelming diversity in the hierarchical nanostructural organization of lepidopteran wing scales. Here, we present a time-resolved, comparative developmental study of hierarchical scale nanostructures in *Parides eurimedes* and five other papilionid species. Our results uphold the putative conserved role of F-actin bundles in acting as spacers between developing ridges, as previously documented in several nymphalid species. Interestingly, while ridges are developing in *P. eurimedes*, plasma membrane manifests irregular mesh-like crossribs characteristic of Papilionidae, which delineate the accretion of cuticle into rows of planar disks in between ridges. Once the ridges have grown, disintegrating F-actin bundles appear to reorganize into a network that supports the invagination of plasma membrane underlying the disks, subsequently forming an extruded honeycomb lattice. Our results uncover a previously undocumented role for F-actin in the morphogenesis of complex wing scale nanostructures, likely specific to Papilionidae.

Key Words: Butterfly Scale, Biological Nanostructure, Hierarchical Morphogenesis, Structural Coloration, F-Actin Reorganization, Plasma Membrane Invagination

Introduction

The patterning and coloration of butterfly wings have been a paradigmatic research focus due to their fundamental role in signalling and crypsis (Beldade and Brakefield, 2002; Sweeney et al., 2003; Tsai et al., 2020). Significant advances have been made recently in identifying the cellular and molecular basis of lepidopteran pigmentary coloration (Matsuoka and Monteiro, 2018; Nadeau et al., 2016; Nishikawa et al., 2015; Reed et al., 2011; Van Belleghem et al., 2023; Zhang et al., 2017a). A small number of regulatory genes have been found to exert significant influence on the synthesis and spatial expression of pigments, as well as regulating cuticle deposition, thereby affecting the overall scale morphology (e.g., Banerjee et al., 2022; Ficarrotta et al., 2022; Matsuoka and Monteiro, 2018; Prakash et al., 2022; Van Belleghem et al., 2023; Wee et al., 2022). For instance, suppression of the *optix* gene has been found to tune lower lamina thickness, inducing iridescent structural coloration and affecting cuticular coverage of the upper lamina (Wasik et al., 2014; Zhang et al., 2017b).

Building on the classic studies on cellular organization of lepidopteran scales (Ghiradella, 1974; Ghiradella, 1985; Ghiradella, 1989; Ghiradella and Radigan, 1976; Overton 1966), a few recent studies utilized advances in microscopy techniques to interrogate the formation of longitudinal ridges (Day et al., 2019; Dinwiddie et al., 2014; McDougal et al., 2021). These insights are, however, limited to ridge formation on the scale surface. Moreover, contemporary research on scale cell development focuses on just a few model taxa (*Bicyclus*, *Precis*, *Heliconius*, *Vanessa*) all from the family of Nymphalidae (Beldade and Brakefield, 2002; Day et al., 2019; Dinwiddie et al., 2014; Matsuoka and Monteiro, 2018; Nadeau et al., 2016; Pomerantz et al., 2020; Prakash et al., 2021; Reed et al., 2011; Sweeney et al., 2003; Van Belleghem et al., 2023;

Wasik et al., 2014; Zhang et al., 2017b), despite an overwhelming diversity in the hierarchical organization of scale nanostructures across Lepidoptera (Ghiradella, 1984; Ghiradella, 1985; Ghiradella, 1989; Prum et al., 2006). A rare exception is the recent work on pierid butterfly *Colias* identifying *bric à brac* as a genetic switch that suppresses UV-reflecting Christmas-tree like ridge gratings in males (Ficarrotta et al., 2022), even though the precise development of the ridge grating is still unresolved (Ghiradella, 1974). Deciphering the cellular and developmental basis of scale organization in beyond just a few model lepidopterans is also highly relevant to current challenges in the synthesis of complex sub-micron and micron-scale hierarchical nanostructures, and could inspire novel biomimetic routes to fabricate multifunctional nanomaterials (Kolle et al., 2010; Pokroy et al., 2009; Potyrailo et al., 2007; Siddique et al., 2017).

The *bauplan* of lepidopteran wing scales consists an ornamented upper lamina over a relatively unstructured basal lamina, supported by arches with pillar-like struts called trabeculae (Ghiradella, 1984) (Fig. S1). The upper lamina comprised of longitudinal ridges with transverse crossribs framing a set of rectilinear windows. These windows typically open into the interior lumen of the scale cell, but can also be covered by a thin layer of cuticular lamina (Ghiradella, 1984). The sides of the ridges feature microribs – fine flute-like stripes visible at higher magnifications under an electron microscope (Fig. S1).

Among all Lepidoptera families, swallowtail butterflies (Papilionidae) not only encompasses the known diversity of scale nanostructure, but also exhibits some of the most complex hierarchical morphologies found in nature (Ghiradella, 1984; Ghiradella, 1985; Ghiradella, 1989; Prum et al., 2006; Saranathan et al., 2010) (Fig. S1). Despite having a few model species (*e.g.*, *Papilio xuthus*, *P. polytes* and *P.*

machaon), the focus of current research on papilionids is limited to molecular basis of mimicry of pigment patterns (e.g., H. et al., 2015; Yoda et al., 2021). The wing scales of papilionid species (*e.g.*, *Parides sesostris*, *Papilio nireus*) exhibit irregular veins or mesh-like crossribs, often with an underlying honeycomb-like lattice of cuticular walls enclosing columnar pores (Ghiradella, 1984; Ghiradella, 1985; Ghiradella and Radigan, 1976; Prum et al., 2006; Saranathan et al., 2010; Wilts et al., 2014) (Figs. 1, and S1). In the following, we use “honeycomb lattices” to refer to irregular crossribs with lattice walls extending into the interior lumen (*e.g.,* green scales in *P. sesostris*, *P. arcas* and *P. eurimedes*), and “irregular crossribs” for crossribs that lack such extruded cuticular walls. In any case, these irregular crossribs are an autapomorphy of Papilionid butterflies (Ghiradella, 1984; Ghiradella, 1985; Ghiradella and Radigan, 1976) that are thought to increase the surface area over which pigments such as papiliochromes can be deposited (Wilts et al., 2014), and likely play a role in thermoregulation as they are efficient absorbers of solar radiation (Siddique et al., 2017).

Here, we use scanning electron microscopy (SEM), conventional confocal and super-resolution Structured Illumination Microscopy (3D-SIM) to study the time-resolved development of hierarchical scale nanostructures in wing scales of six papilionid species, chiefly in *Parides eurimedes*. We discovered that following ridge formation, rows of chitinous disks form in between the ridges, followed by disintegration of F-actin that reorganizes into a mesh-like network. This network likely acts as a template for subsequent formation of honeycomb lattices by driving plasma membrane invagination into the scale lumen. Our study uncovers a novel process of wing scale nanostructure formation in Papilionid species.

Results

Wing scale ridge formation is conserved in Papilionidae

We comparatively studied the wing scale growth in *Papilio polytes* and *Parides eurimedes,* which have irregular crossribs and honeycomb lattices respectively. Early stages of scale cell growth are as previously documented in several nymphalid species (Day et al., 2019; Dinwiddie et al., 2014; Ghiradella, 1974; Pomerantz et al., 2020). Wheat germ agglutinin (WGA) stains the plasma membrane during early stages of scale development in *P. eurimedes*. Scale cells from relatively young pupae at 38% development resemble elongated buds containing densely packed polymerizing F-actin filaments (Fig. S2A-A" and B-B"). At 43% development, F-actin filaments form thicker bundles that extend down the full length of scale cells (Fig. S2C'), laying down a scaffold that determines the eventual position of ridges (Dinwiddie et al., 2014). WGA stains pleating membranes (longitudinal striations) in between adjacent rows of F-actin bundles (Fig. S2C-C" and D-D"). Around 48% to 50% development, the developing ridges can be more clearly discerned in between F-actin bundles (Fig. S2E-E", S15D-D" and E-E"). At this stage, there also appears to be irregular gaps in WGA staining in between the ridges of *P. eurimedes* scales (Fig. S2E). These vein-like features resemble the irregular crossribs seen in adult wing scales (Fig. 1B-C, Fig. S15B-C).

Cross-rib and cuticular disk formation in Parides eurimedes

We use lectin and membrane stains to follow plasma membrane topology and cuticle deposition during scale cell maturation (Figs. 2, and S3-S6). At 48% development, plasma membrane appears mottled while WGA predominantly stains longitudinal striations that will become ridges (Figs. 2A-C, and S3B-B"). In cross-sections, both stains appear to be in close contact at the periphery of the cell, with

145 plasma membrane underlying the cuticular layer (Figs. 2C and S3C-C''). This
146 observation is expected, as the cuticle of extracellular origin is being deposited onto
147 the scale cell membrane. At 52% pupal development, plasma membrane shows
148 distinct pleating corresponding to the developing ridges, with irregular crossribs in
149 between (Figs. 2A'-C', and S4A'-C'). The bulk of cuticle remains above the plasma
150 membrane at this stage (Figs. 2C', and S4C''). At around 62% pupal development,
151 ridges appear to have grown to their near final configuration while lectin staining
152 reveals planar, disk-like cuticular features (hereafter cuticular disks) arranged in rows
153 in between the ridges (Figs. 2A''-C'', 2A'''-C''', S5 and S6).
154
155 *Dynamics of F-actin reorganization in Parides eurimedes*
156 We also co-stain chitin and F-actin on the developing pupal scales to
157 investigate the role of cytoskeleton in scale nanostructure formation. Interestingly, as
158 cuticular disks of various sizes are forming in between ridges at 57% development, F-
159 actin bundles are breaking down into short fibrils distributed around the disks (Figs.
160 3B-C, and S7 and movie S1). As the scales became more sclerotized and flattened
161 out at 67% development, disintegrating F-actin appears to reorganize and associate
162 more clearly with cuticular disks, which now appear elongated and slightly tubular in
163 cross-sectional view (Figs. 3A'-C', S8 and movie S2). By 76% development, the
164 cuticular disks appeared hollow, and are surrounded by distinct bulb-like structures
165 formed by the disintegrated F-actin bundles (Figs. 3A''-C'', S9 and movie S3).
166 To better understand the mechanism behind F-actin reorganization, we
167 investigated whether the actin-related proteins, Arp2/3 complex, is a potential factor
168 regulating the dendritic growth of actin fibrils (Hudson and Cooley, 2002; Pollard, 2007;
169 Rouiller et al., 2008). At around 52% development in *P. eurimedes*, Arp2/3 complex

appear in a sparse punctate pattern while the F-actin bundles are still intact (Figs. 4A-C, and S10). As F-actin bundles disintegrate and start to reorganize around 62% development, a relatively higher density of punctate Arp2/3 complex is seen in close association with the F-actin network (Figs. 4A'-C', and S11). At a later stage (~76% development), no distinctive punctate patterns can be discerned (Figs. 4A"-C", and S12), which is expected given that the reorganization of F-actin is nearly complete by this stage (see Fig. 3). However, the scales are more mature at this point with prominent ridges, and autofluorescence signal from the cuticle has shifted into the green wavelengths (Fig. S13), complicating the interpretation of the Arp2/3 immunofluorescence signal.

Pharmacological disruption of Arp2/3 using CK-666

In order to mechanistically test the putative role of Arp2/3 in reorganizing F-actin during honeycomb lattice formation, we carried out pharmacological disruption experiments in pupae of both *Parides* and *Papilio* species using CK-666, a known inhibitor of the Arp2/3 complex (Henson et al., 2015). Unfortunately, we were only able to obtain a small number of *Parides* pupae, which were already somewhat mature when they arrived, and further, a third of the pupae were dead on arrival (Table S1). Honeycomb lattices can be seen in scales from emerged males of both *P. eurimedes* and *P. iphidamas* pupae treated with CK-666 (Fig. S14). However, the height of the honeycombs in scales from pupae treated on 52% development were on average lower than the control (Figs. S14A and D). Furthermore, in *P. eurimedes*, the height of the honeycombs in scales from pupae injected at 57% development were higher on average than those treated at 52% development, but indistinguishable from any controls (Fig. S14A). These results are reminiscent of a previous study utilizing

195 cytochalasin-D to inhibit linear actin polymerization (Dinwiddie et al., 2014) that found
196 that once the pupae were past a certain developmental stage, ridge formation is no
197 longer disrupted by the inhibitor. However, despite this intriguing trend in our results
198 being consistent with a hypothesized role for Arp2/3, we require data with robust
199 sample sizes and younger time points (*i.e.* 28%-48% development) for *Parides spp.* in
200 future experiments to validate the role of Arp2/3.

201 We also injected CK-666 into the wing pouches of the more readily available
202 *Papilio polytes* pupae from 40%-80% development to cover the possible timeframe
203 during which Arp2/3 complex could be involved in F-actin reorganization. However,
204 neither cuticular disks nor the dendritic reorganization of linear F-actin bundles are
205 observed in *P. polytes*, whose adult scales have irregular crossribs without the deep
206 lattice walls, *i.e.*, no honeycombs (Fig. S15B and C). Shortly after ridge formation at
207 60% development (Fig. S15 D-D''), irregular crossribs are seen in between intact F-
208 actin bundles (Fig. S15 F-F''). At 70% development, strong chitin autofluorescence
209 signal is seen at the ridges (Fig. S15 H-I). Since F-actin reorganization is absent in
210 this species, Arp2/3 inhibition did not disrupt ridge and crossrib formation in *P. polytes*
211 as expected (Fig. S16). Concurrent SEM imaging of pupal scales from the same
212 samples show the formation of irregular crossribs is similarly not affected (Fig. S17).
213 Our results suggests the formation of cuticular disks and their subsequent extrusion
214 by reorganizing F-actin is restricted to species with elaborate honeycomb lattice walls
215 such as *Parides eurimedes*.

216

217 *Honeycomb morphogenesis is conserved across Papilionidae*

218 We also assayed the development of pupal wing scales of several other
219 papilionid species: *Parides arcas*, *Papilio nireus, and Papilio palinurus,* (Fig. 5),

220 Although we were unable to obtain pupae with clearly marked pupation dates for these
221 three species, we observed similar early stages of honeycomb development as seen
222 in *P. eurimedes*. In adult male *P. arcas*, green scales have well developed honeycomb
223 lattice walls that sit above single gyroid crystals (Fig. 5A). During *P. arcas* pupal scale
224 development, both solid and hollow (annular) cuticular disks can be observed in
225 between intact linear actin bundles (Fig. 5B-B' and C-C'). The same is observed in *P.*
226 *nireus*, where the upper lamina of adult blue scales consists of an elaborate
227 honeycomb lattice with smaller sized pores (Fig. 5D, E and F). In *P. palinurus* adults,
228 green forewing cover scales feature large concave depressions in between the ridges
229 (Fig. 5G). Phalloidin staining of pupal *P. palinurus* scales reveals reorganization of
230 longitudinal F-actin bundles into a shallow concave network (concentric rings in cross-
231 section) (Figs. 5H-I, and Movie S4), which closely correspond to the cuticular dimples
232 seen in adult green cover scales.
233

234 **Discussion**

235 Swallowtail butterflies (Papilionidae) is the sister lineage to all other butterflies
236 (Espeland et al., 2018) and the showcase family of lepidopterans, as they exhibit some
237 of the most diverse assortment of wing scale nanostructures (Ghiradella, 1985; Prum
238 et al., 2006). Papilionid wing scales generally exhibit irregular crossribs, with some
239 having underlying cuticular walls enclosing tubular pores, although the regularity and
240 depth of the walls vary between species (Fig. S1). These crossrib patterns are unlike
241 the regular, rectilinear crossribs commonly seen in other lepidopteran families, *e.g.*,
242 Nymphalidae (Fig. S1R). In this study, we extended previous observations that parallel
243 F-actin bundles configure the spacing and position of longitudinal ridges of wing scales
244 (Day et al., 2019; Dinwiddie et al., 2014; Ghiradella, 1974; Pomerantz et al., 2020) to

245 Papilionidae, further supporting the hypothesis that this mechanism is broadly
246 conserved across lepidopterans.

247 Our first novel finding is the appearance of irregular crossrib patterns in the
248 plasma membrane between surface ridges, which seemed to serve as a template for
249 chitin accretion into chitinous disks. This process is important as it marks the beginning
250 of honeycomb lattice formation. Further, our results revealed that F-actin plays a
251 predominant and previously unconsidered role in the morphogenesis of some
252 papilionid butterfly wing scales. Once the longitudinal ridges have developed, F-actin
253 bundles, which typically degenerate in nymphalid species (Day et al., 2019; Dinwiddie
254 et al., 2014), subsequently reorganize into a reticulate network surrounding rows of
255 cuticular disks on the scale surface. This actin network likely draws in plasma
256 membrane underlying the cuticular disks into a porous honeycomb lattice. Similar non-
257 linear F-actin morphologies have been observed in other organisms. In diatoms, F-
258 actin organizes into an interdigitating mesh-like porous network during development
259 (Tesson and Hildebrand, 2010). This actin network defines frustule (cell walls)
260 morphogenesis by providing a template for silica biomineralization at the meso and
261 micro scales. In mammalian cells, transient ring-like F-actin structures are thought to
262 drive autophagosome generation by serving as a scaffold for mitophagy initiation
263 structures. 3D-SIM revealed F-actin partially associating with mitochondria in the form
264 of curved sheet (Hsieh and Yang, 2019), akin to the F-actin structures seen in this
265 study.

266 The schematic in Figure 6 illustrates our proposed formation of honeycomb
267 lattices in some Papilionid wing scales. During early stages of scale formation, F-actin
268 bundles prefigure the loci of future ridge formation in between adjacent actin bundles
269 (Dinwiddie et al., 2014). Plasma membrane then forms a scaffold resembling the

270 irregular crossrib pattern. The cuticle accretes into roughly circular disks delineated by
271 the scaffold. Reorganization of F-actin around the chitinous disks draws the plasma
272 membrane along with the overlying cuticle inwards, moulding it into the lengthened
273 cuticular walls of the honeycomb lattice.

274 In our attempt to unravel the molecular players in actin reorganization, we used
275 CK-666 to inhibit the role of Arp2/3 complex in actin branching (Henson et al., 2015).
276 However, CK-666 did not quite disrupt the formation of honeycombs even when
277 administered across multiple timepoints. A variety of reasons could potentially explain
278 this. While 100uM of CK-666 has been shown to work in other animal models (Henson
279 et al., 2015), it might still not be a sufficient titre for papilionid butterfly pupal scales.
280 Unfortunately, due to logistical difficulties in obtaining and rearing *Parides spp.*, we
281 were unable to perform a thorough optimization using CK-666. Furthermore, the
282 *Parides* pupae were likely too mature at the time of CK-666 treatment, when the F-
283 actin network has already been established (52% development). In a recent study
284 (Sakamoto et al., 2018), CK-666 did not disrupt the formation of cortical actin
285 meshwork in Sertoli cells of mouse seminiferous tubules, as they were found to be
286 regulated by formins rather than Arp2/3. This suggests that other molecular players,
287 including formins, could be involved in wing scale honeycomb morphogenesis and
288 needs testing.

289 We note that the irregular crossrib patterns are in place while the ridges are still
290 growing (Fig. 2A'-C'). These crossribs appear to constrain and delineate the
291 accumulation of cuticle into planar disks in between the ridges. A close examination
292 of SEM images (Figs. 1B and S1) reveals that the endpoints of crossribs at the ridge
293 interface are often connected to microribs present on the ridges. Given their relatively
294 small size and pitch, we are unable to resolve the development of microribs here,

which likely requires imaging techniques with even higher resolution such as Photo-activated localization microscopy (PALM) and stochastic optical reconstruction microscopy (STORM). However, both the periodic stripes (microribs) and quasi-periodic spots (crossribs) are reminiscent of Turing patterns (Meinhardt, 1982; Turing, 1952), *i.e.*, implying that an activator-inhibitor type mechanism could be involved in their formation. Alternatively, the crossrib pattern could be as a result of Ostwald ripening or phase separation-like processes leading to stable, quasi-periodic, foam-like perforations on the plasma membrane in between ridges (Elson et al., 2010; Rosetti et al., 2017; Voorhees, 1985).

Overall, the presence of chitinous disks followed by F-actin reorganization appears to be specific to species with extended honeycomb lattice walls, *e.g. Parides eurimedes, Parides arcas*, and *Papilio nireus* (Fig. S1A and S1E). Such reorganized actin structures are not observed in species with shallow irregular crossribs, such as *P. polytes* (Fig. S15). On the other hand, several *Papilio* species (*e.g.*, *palinurus*, *blumei*, *karna*) possess structurally-colored cover scales (Ghiradella; Prum et al., 2006) with widely spaced and reduced (in both height and number) ridges. These scales have no apparent crossribs, trabeculae or honeycombs. Instead, they have a characteristic inter-ridge array of concave depressions and underlying perforated lamellae in the scale interior (Fig. S1L and M). Based on our observations, we speculate that the dimpled appearance of cover scales is templated by reorganization of F-actin bundles into a whorl-like concave network. This could represent an extreme modification of the proposed developmental program of the usual papilionid honeycomb lattice. Without crossribs, the pore sizes of honeycombs are likely constrained only by the pitch of the ridges. This is consistent with our observation that the outermost F-actin rings possess dimensions approaching the inter-ridge distance

320 (Fig. 5C). Without the trabeculae, the lumen multilayer fills the entire interior of the
321 scale right up to the shallow dimples.

322 Interestingly, in typical lepidopteran scale cells, the trabeculae extend
323 downwards from the crossribs and form columns of arches in between the ridges
324 (Ghiradella, 1974; Ghiradella, 1985; Ghiradella, 1989; Ghiradella and Radigan, 1976;
325 Overton 1966), suggesting they are developmentally connected. Recently, Matsuoka
326 and Monteiro (2018) found that *DDC* mutant of *Bicyclus anynana* (Nymphalidae)
327 possessed irregularly-spaced and thin crossribs with sheet-like vertical trabeculae
328 instead of feet-like, arched trabeculae (see Fig. 4A of (Matsuoka and Monteiro, 2018)).
329 These mutant scale morphologies are somewhat reminiscent of the irregular crossribs
330 and honeycomb lattice walls of Papilionidae. This suggests spatio-temporal changes
331 in expression patterns of single genes such as *DDC* could possibly alter crossrib
332 morphology and drive honeycomb formation. However, any putative pleiotropic role of
333 pigment-pathway genes in organizing papilionid scale morphology should be
334 reconciled with that of actin reorganization. Future studies could look at knocking out
335 *DDC* and other pigment-pathway genes during papilionid pupal development, in
336 addition to inhibiting actin-binding proteins including Arp2/3 and formins, and tinkering
337 with master regulatory genes like *optix* (Banerjee et al., 2022; Wasik et al., 2014;
338 Zhang et al., 2017b).

339 The smooth endoplasmic reticulum (SER) has been implicated in templating
340 luminal scale nanostructures during pupal development. Given that the papilionid
341 honeycomb lattice extends into the lumen of the scale cells, any putative role of the
342 SER in honeycomb morphogenesis should also be investigated. It would be of interest
343 to follow the development of pupal wing scales using tissue clearing techniques or
344 attempt a more finely resolved developmental time series to capture the full complexity

345 of molecular and cytoskeletal dynamics. Comparatively understanding the
346 morphogenesis of hierarchical nanostructures across biodiversity could inspire facile,
347 biomimetic routes to synthesizing hierarchically structured materials for technological
348 applications, given current challenges in the engineering of complex multi-functional
349 mesophases (Kolle et al., 2010; Pokroy et al., 2009; Potyrailo et al., 2007; Siddique et
350 al., 2017).
351

352 **Materials and Methods**

353 *Experimental design*

354 To understand the process of scale nanostructure formation, we performed time-
355 resolved imaging on developing pupal scales using specific biomarkers conjugated
356 with fluorophores. Since cellular membranes and cytoskeletal elements have been
357 identified as key components driving scale cell development, we used biomarkers
358 targeting F-actin, cuticle (chitin), plasma membrane and Arp2/3 complex. We used 3D
359 structured illumination microscope (3D-SIM) and lattice SIM to try and resolve
360 structures beyond the diffraction limit. We would have preferred to present all confocal
361 and SIM data solely on a single patch, for instance, the green dorsal forewing cover
362 scales of pupal *P. eurimedes*. However, for time points where scales were highly
363 crumpled or folded, we addressed this gap with data from black areas adjacent to the
364 green patch, or from homologous yellow dorsal forewing patch on females. The overall
365 consistency of the results validates our approach.
366

367 *Dissection of pupae and tissue preparation*

368 Pupae were purchased in multiple batches from Marl Insect and Butterfly Culture
369 (Philippines), Stratford-upon-Avon Butterfly Farm (UK), and Mariposario del Bosque

370 Nuevo (Costa Rica) between June 2017 - April 2021. Precise pupation dates were
371 available for *Papilio polytes* and one batch of *P. eurimedes* pupae. For batches without
372 information on the pupation dates, we estimate the rough pupation stage (indicated by
373 ~, *e.g.*, Figs. 2A'''-C''', and 4) by morphological comparisons to this batch. Sex of each
374 pupa was determined by examining markings on the ventral segments. Wings from
375 each pupa were dissected in cold Phosphate Buffer Saline (PBS) and immediately
376 fixed in 4% PEM-PFA at room temperature for 15 mins. Following washes in PBS,
377 wings were placed in blocking buffer (0.5% NP-40) at 4ºC overnight prior to staining.
378 The average duration from pupation to emergence is 10 days for *P. polytes* and 21
379 days for *P. eurimedes*. We report the percentage of development in our time series for
380 ease of comparison between species with different developmental rates.
381
382 *Developmental time series with Wheat Germ agglutinin, phalloidin and anti-Arp2*
383 Wheat Germ Agglutinin (WGA) was previously used to visualize butterfly scale cell
384 growth and is thought to initially stain plasma membrane before switching to chitin at
385 later developmental stages (Dinwiddie et al., 2014). Phalloidin is a standard method
386 to visualize F-actin. For AF-555 WGA and AF-647 phalloidin double-staining, pupal
387 wings were incubated in 1:200 dilution of Alexa Fluor 555-conjugated WGA (Invitrogen
388 W32464) and 1:40 dilution of Alexa Fluor 647-conjugated phalloidin (Invitrogen
389 A22287) for an hour at room temperature. For FITC WGA and TRITC phalloidin double
390 staining, *P. palinurus* pupal wings were incubated in 1:100 dilution of FITC WGA (EY
391 Labs F-2101-5) and 1:100 dilution of TRITC phalloidin (Sigma P1951) for an hour at
392 room temperature. Arp2 is the ATP-binding component of the actin Arp2/3 complex,
393 which functions as an actin nucleator in branched actin networks (Goley and Welch,
394 2006; Smith et al., 2013). After blocking, pupal wings were incubated with a 1:500

395 dilution of rabbit anti-Arp2 (Abcam ab47654; pblast search revealed Uniprot #P61160,
396 Human Arp2 has 82% sequence similarity to XP_013178655.1, *Papilio xuthus Arp2*)
397 at 4℃ overnight. After washing, the wings were incubated in buffer with a 1:300 dilution
398 of Alexa Fluor 594 Goat anti Rabbit secondary antibody (Abcam ab150088) for an
399 hour at room temperature.
400
401 *Time series with CellMask Plasma Membrane stain*
402 As the CellMask plasma membrane stain does not survive permeabilization, dissected
403 pupal wings were immediately stained with a 1:300 dilution of CellMask Deep Red
404 (Invitrogen C10046) for 10 mins. After removing the staining solution, the wings were
405 fixed in 4% PEM-PFA at room temperature for 15 mins. Following washes in PBS,
406 pupal wings were stained with a 1:200 dilution of Alexa Fluor 555-conjugated WGA
407 (Invitrogen W32464) for an hour at room temperature. In order to prevent
408 permeabilization, the buffers for Cellmask stains did not contain any detergents (e.g.
409 Triton).
410
411 *Arp2/3 inhibition with CK-666*
412 CK-666 was purchased from Sigma Aldrich (SML0006) and the stock solution was
413 dissolved in DMSO. For pupal injections, CK-666 was diluted in 1x Grace's insect
414 medium to final concentration of 100μM. Two to three P. polytes pupae were injected
415 with CK-666 at 40%, 50%, 60%, 70%, and 80% development. Around 8-10μL of CK-
416 666 is injected into wing pouches using a glass needle. Control pupae were injected
417 with equal volume of DMSO diluted in Grace's insect medium. All injected pupae were
418 dissected at 80% development and stained for immunofluorescence. Pupae injected
419 on 80% development were allowed to develop for at least two hours before dissection.

420

421 *Negative controls*

422 For experiments with non-fluorophore-conjugated primary antibodies (Arp2 staining),
423 we labelled a separate wing from the same individual with the secondary antibody only.
424 This is to determine if the observed fluorescence signal is due to non-specific binding
425 of secondary antibodies. After blocking, pupal wings were incubated without primary
426 antibodies (only buffer) at 4℃ overnight. After washing, the wings were incubated with
427 a 1:300 dilution of Alexa Fluor 594 Goat anti Rabbit secondary antibody (Abcam
428 ab150088) for an hour at room temperature. Negative controls were imaged using the
429 same settings (laser power, gain, *etc.*) as the anti-*Arp2* antibody-stained test samples.

430

431 *Image acquisition, data processing*

432 Following washes, the wings were mounted on glass slides in Prolong Gold antifade
433 (Life Technologies P36930), covered with #1 thickness coverslips and sealed with nail
434 polish. Confocal images were acquired using Olympus FV3000 (60x), Nikon A1R
435 (100x) and Leica SP8 (100x). 3D-SIM was performed on a DeltaVision OMX and
436 lattice SIM using Zeiss Elyra 7. Confocal data acquired with Olympus FV3000 and
437 Nikon A1RSIM data were deconvolved using default settings in Huygens Professional
438 v20.04. Confocal data acquired with Leica SP8 were deconvolved using default
439 settings in Leica's Lightning deconvolution software during acquisition. All images
440 were examined and processed using Bitplane Imaris Viewer 9.5.1. Movies were
441 generated using Bitplane Imaris and edited using Shotcut v19.07.15 (Meltytech, LLC)

442

443 *Critical point drying (CPD)*

444 Wings from each pupa were dissected in cold PBS and immediately fixed in 4% PEM-
445 PFA at room temperature for 15 mins. Following washes in PBS, wings were subjected
446 to serial dehydration in 25%, 50%, 70%, 90% and absolute ethanol for 10 minutes
447 each. The specimens were then transferred to the sample holders and dried using
448 Leica EM CPD300 Automated Critical Point Dryer with the following settings: (CO2
449 influx) Medium speed, 120s delay; (Exchange process) Speed 5, 14 cycles; Medium
450 heating speed; and Medium gas out speed. It should be note that direct air drying of
451 soft samples *e.g.* pupal wing scales is not recommended, as water surface tension
452 forces will result in significant distortion of specimen structure (Bray et al., 1993).
453
454 *Conventional and focused ion beam (FIB) scanning electron microscopy (SEM)*
455 Adult scales were individually picked with a needle and placed on carbon tape.
456 Mounted scales were fractured using a razor-blade to obtain cross-sectional views. All
457 samples were sputter-coated with platinum or gold to increase conductivity and reduce
458 charging. Samples were imaged using JEOL JSM 6010LV Scanning Electron
459 Microscope at 15-20k.
460
461 For focused ion beam (FIB) milling, samples were prepared by sputter-coating with
462 platinum to increase conductivity. The sectioned scale shown in Fig. 1C is milled using
463 a gallium ion beam on a FEI Versa 3D with the following settings: beam voltage - 8kV,
464 beam current - 12pA at a 52° tilt. Image acquisition was performed in the same
465 equipment with the following settings: beam voltage - 5kV, beam current - 13pA.
466
467

Acknowledgements:

We are indebted to Antonia Monteiro for generously providing us with lab resources, including the use of insectary. We thank Cédric Finet for sharing FIB-SEM image of *P. eurimedes*. We are grateful to the Monteiro lab, C. Finet, Cynthia He, Rong Li, Sasha Bershadsky, and Dan Morse for their thoughtful suggestions. We thank Sree Vaishnavi Sundararajan and Gianluca Grenci (MBI) for access and help with SEM, Tong Yan (CBIS), Mak Kah Jun and Peng Qiwen (MBI), Laura and Keshmarathy Sacadevan (Singhealth Advanced Bioimaging) for help with confocal microscopy, Graham Wright and Goh Wah Ing (A*STAR AMP) and Shi Xianke (Zeiss) for help with SIM data acquisition.

Funding: This work was supported by a Graduate Research Excellence Grant - Rosemary Grant Advanced Award from SSE to K.S., Yale-NUS startup funds (R-607-261-182-121) and a Singapore NRF CRP Award (CRP20-2017-0004) to V.S.

Author Contributions: V.S. and K.S. designed the study. K.S. performed the experiments. Both authors analyzed the results and wrote the manuscript.

Competing interests: Authors declare no competing interests.

References

Banerjee, T. D., Kwi-Shan, S. and Monteiro, A. (2022). Reuse of a wing venation gene-regulatory network in patterning the eyespot rings of butterflies. *BioRxiv*, 2021.05.22.445259.

Beldade, P. and Brakefield, P. M. (2002). The genetics and evo-devo of butterfly wing patterns. *Nat Rev Genet* 3, 442-52.

Bray, D. F., Bagu, J. and Koegler, P. (1993). Comparison of hexamethyldisilazane (HMDS), Peldri II, and critical-point drying methods for scanning electron microscopy of biological specimens. *Microsc Res Tech* 26, 489-495.

Day, C. R., Hanly, J. J., Ren, A. and Martin, A. (2019). Sub-micrometer insights into the cytoskeletal dynamics and ultrastructural diversity of butterfly wing scales. *Developmental Dynamics* 248, 657-670.

Dinwiddie, A., Null, R., Pizzano, M., Chuong, L., Leigh Krup, A., Ee Tan, H. and Patel, N. H. (2014). Dynamics of F-actin prefigure the structure of butterfly wing scales. *Dev Biol* 392, 404-18.

Elson, E. L., Fried, E., Dolbow, J. E. and Genin, G. M. (2010). Phase Separation in Biological Membranes: Integration of Theory and Experiment. *Annual Review of Biophysics* 39, 207-226.

Espeland, M., Breinholt, J., Willmott, K. R., Warren, A. D., Vila, R., Toussaint, E. F. A., Maunsell, S. C., Aduse-Poku, K., Talavera, G., Eastwood, R. et al. (2018). A Comprehensive and Dated Phylogenomic Analysis of Butterflies. *Current Biology* 28, 770-778.e5.

Ficarrotta, V., Hanly, J. J., Loh, L. S., Francescutti, C. M., Ren, A., Tunstrom, K., Wheat, C. W., Porter, A. H., Counterman, B. A. and Martin, A. (2022). A genetic switch for male UV iridescence in an incipient species pair of sulphur butterflies. *Proc Natl Acad Sci U S A* 119.

Ghiradella, H. (1974). Development of ultraviolet-reflecting butterfly scales: How to make an interference filter. *Journal of Morphology* 142, 395-410.

Ghiradella, H. (1984). Structure of Iridescent Lepidopteran Scales - Variations on Several Themes. *Annals of the Entomological Society of America* 77, 637-645.

514 Ghiradella, H. (1985). Structure and development of iridescent lepidopteran scales: the
515 Papilionidae as a showcase family. *Annals of the Entomological Society of America* 78, 252-264.
516 Ghiradella, H. (1989). Structure and development of iridescent butterfly scales: Lattices and
517 laminae. *Journal of Morphology* 202, 69-88.
518 Ghiradella, H. and Radigan, W. (1976). Development of butterfly scales. II. Struts, lattices and
519 surface tension. *J Morphol* 150, 279-297.
520 Goley, E. D. and Welch, M. D. (2006). The ARP2/3 complex: an actin nucleator comes of age.
521 *Nature reviews. Molecular cell biology* 7, 713-26.
522 H., N., Iijima, T., R., K., Yamaguchi, J., Ando, T., Suzuki, Y., S., S., Fujiyama, A., Kosugi, S.,
523 Hirakawa, H. et al. (2015). A genetic mechanism for female-limited Batesian mimicry in Papilio
524 butterfly. *Nat. Genet.*
525 Henson, J. H., Yeterian, M., Weeks, R. M., Medrano, A. E., Brown, B. L., Geist, H. L., Pais, M.
526 D., Oldenbourg, R. and Shuster, C. B. (2015). Arp2/3 complex inhibition radically alters lamellipodial
527 actin architecture, suspended cell shape, and the cell spreading process. *Molecular Biology of the*
528 *Cell* 26, 887-900.
529 Hsieh, C. W. and Yang, W. Y. (2019). Omegasome-proximal PtdIns(4,5)P(2) couples F-actin
530 mediated mitoaggregate disassembly with autophagosome formation during mitophagy. *Nat*
531 *Commun* 10, 969.
532 Hudson, A. M. and Cooley, L. (2002). A subset of dynamic actin rearrangements in
533 Drosophila requires the Arp2/3 complex. *J Cell Biol* 156, 677-87.
534 Kolle, M., Salgard-Cunha, P. M., Scherer, M. R. J., Huang, F. M., Vukusic, P., Mahajan, S.,
535 Baumberg, J. J. and Steiner, U. (2010). Mimicking the colourful wing scale structure of the Papilio
536 blumei butterfly. *Nature Nanotechnology* 5, 511-515.
537 Matsuoka, Y. and Monteiro, A. (2018). Melanin Pathway Genes Regulate Color and
538 Morphology of Butterfly Wing Scales. *Cell Rep* 24, 56-65.

539 McDougal, A. D., Kang, S., Yaqoob, Z., So, P. T. C. and Kolle, M. (2021). In vivo visualization of
540 butterfly scale cell morphogenesis in Vanessa cardui. *Proc Natl Acad Sci U S A* 118.
541 Meinhardt, H. (1982). Models of Biological Pattern Formation. London: Academic Press.
542 Nadeau, N. J., Pardo-Diaz, C., Whibley, A., Supple, M. A., Saenko, S. V., Wallbank, R. W. R.,
543 Wu, G. C., Maroja, L., Ferguson, L., Hanly, J. J. et al. (2016). The gene cortex controls mimicry and
544 crypsis in butterflies and moths. *Nature* 534, 106-110.
545 Nishikawa, H., Iijima, T., Kajitani, R., Yamaguchi, J., Ando, T., Suzuki, Y., Sugano, S., Fujiyama,
546 A., Kosugi, S., Hirakawa, H. et al. (2015). A genetic mechanism for female-limited Batesian mimicry in
547 Papilio butterfly. *Nat Genet* 47, 405-409.
548 Overton , J. (1966). MICROTUBULES AND MICROFIBRILS IN MORPHOGENESIS OF THE SCALE
549 CELLS OF EPHESTIA KÜHNIELLA. *Journal of Cell Biology* 29, 293-305.
550 Pokroy, B., Kang, S. H., Mahadevan, L. and Aizenberg, J. (2009). Self-organization of a
551 mesoscale bristle into ordered, hierarchical helical assemblies. *Science* 323, 237-40.
552 Pollard, T. D. (2007). Regulation of Actin Filament Assembly by Arp2/3 Complex and Formins.
553 *Annual Review of Biophysics and Biomolecular Structure* 36, 451-477.
554 Pomerantz, A. F., Siddique, R. H., Cash, E. I., Kishi, Y., Pinna, C., Hammar, K., Gomez, D., Elias,
555 M. and Patel, N. H. (2020). Developmental, cellular, and biochemical basis of transparency in the
556 glasswing butterfly Greta oto. *BioRxiv*, 2020.07.02.183590.
557 Potyrailo, R. A., Ghiradella, H., Vertiatchikh, A., Dovidenko, K., Cournoyer, J. R. and Olson, E.
558 (2007). Morpho butterfly wing scales demonstrate highly selective vapour response. *Nat Photon* 1,
559 123-128.
560 Prakash, A., Finet, C., Banerjee, T. D., Saranathan, V. and Monteiro, A. (2022). Antennapedia
561 and optix regulate metallic silver wing scale development and cell shape in Bicyclus anynana
562 butterflies. *Cell Rep* 40, 111052.

563 Prakash, A., Finet, C., Saranathan, V. and Monteiro, A. (2021). Antennapedia regulates
564 metallic silver wing scale development and cell shape in Bicyclus anynana butterflies. *BioRxiv*,
565 2021.10.19.46493.
566 Prum, R. O., Quinn, T. and Torres, R. H. (2006). Anatomically diverse butterfly scales all
567 produce structural colours by coherent scattering. *Journal of Experimental Biology* 209, 749-765.
568 Reed, R. D., Papa, R., Martin, A., Hines, H. M., Counterman, B. A., Pardo-Diaz, C., Jiggins, C.
569 D., Chamberlain, N. L., Kronforst, M. R., Chen, R. et al. (2011). optix Drives the Repeated Convergent
570 Evolution of Butterfly Wing Pattern Mimicry. *Science* 333, 1137-1141.
571 Rosetti, C. M., Mangiarotti, A. and Wilke, N. (2017). Sizes of lipid domains: What do we know
572 from artificial lipid membranes? What are the possible shared features with membrane rafts in cells?
573 *Biochimica et Biophysica Acta (BBA) - Biomembranes* 1859, 789-802.
574 Rouiller , I., Xu , X.-P., Amann , K. J., Egile , C., Nickell , S., Nicastro , D., Li , R., Pollard , T. D.,
575 Volkmann , N. and Hanein , D. (2008). The structural basis of actin filament branching by the Arp2/3
576 complex. *Journal of Cell Biology* 180, 887-895.
577 Sakamoto, S., Thumkeo, D., Ohta, H., Zhang, Z., Huang, S., Kanchanawong, P., Fuu, T.,
578 Watanabe, S., Shimada, K., Fujihara, Y. et al. (2018). mDia1/3 generate cortical F-actin meshwork in
579 Sertoli cells that is continuous with contractile F-actin bundles and indispensable for
580 spermatogenesis and male fertility. *PLoS Biol.* 16, e2004874.
581 Saranathan, V., Osuji, C. O., Mochrie, S. G. J., Noh, H., Narayanan, S., Sandy, A., Dufresne, E.
582 R. and Prum, R. O. (2010). Structure, function, and self-assembly of single network gyroid (I4(1)32)
583 photonic crystals in butterfly wing scales. *Proceedings Of The National Academy Of Sciences Of The*
584 *United States Of America* 107, 11676-11681.
585 Siddique, R. H., Donie, Y. J., Gomard, G., Yalamanchili, S., Merdzhanova, T., Lemmer, U. and
586 Hölscher, H. (2017). Bioinspired phase-separated disordered nanostructures for thin photovoltaic
587 absorbers. *Science Advances* 3, e1700232.

588 Smith, B. A., Daugherty-Clarke, K., Goode, B. L. and Gelles, J. (2013). Pathway of actin
589 filament branch formation by Arp2/3 complex revealed by single-molecule imaging. *Proc Natl Acad*
590 *Sci U S A* 110, 1285-90.
591 Sweeney, A., Jiggins, C. and Johnsen, S. (2003). Insect communication: Polarized light as a
592 butterfly mating signal. *Nature* 423, 31-32.
593 Tesson, B. and Hildebrand, M. (2010). Extensive and intimate association of the cytoskeleton
594 with forming silica in diatoms: control over patterning on the meso- and micro-scale. *PLoS One* 5,
595 e14300.
596 Tsai, C. C., Childers, R. A., Nan Shi, N., Ren, C., Pelaez, J. N., Bernard, G. D., Pierce, N. E. and
597 Yu, N. (2020). Physical and behavioral adaptations to prevent overheating of the living wings of
598 butterflies. *Nat Commun* 11, 551.
599 Turing, A. M. (1952). The chemical basis of morphogenesis. *Philosophical Transactions of the*
600 *Royal Society of London* 237, 37-72.
601 Van Belleghem, S. M., Ruggieri, A. A., Concha, C., Livraghi, L., Hebberecht, L., Rivera, E. S.,
602 Ogilvie, J. G., Hanly, J. J., Warren, I. A., Planas, S. et al. (2023). High level of novelty under the hood of
603 convergent evolution. *Science* 379, 1043-1049.
604 Voorhees, P. W. (1985). The theory of Ostwald ripening. *Journal of Statistical Physics* 38,
605 231-252.
606 Wasik, B. R., Liew, S. F., Lilien, D. A., Dinwiddie, A. J., Noh, H., Cao, H. and Monteiro, A.
607 (2014). Artificial selection for structural color on butterfly wings and comparison with natural
608 evolution. *Proceedings Of The National Academy Of Sciences Of The United States Of America* 111,
609 12109-12114.
610 Wee, J. L. Q., Das Banerjee, T., Prakash, A., Seah, K. S. and Monteiro, A. (2022). Distal-less
611 and spalt are distal organisers of pierid wing patterns. *EvoDevo* 13, 12.

Wilts, B. D., N, I. and Stavenga, D. G. (2014). Pigmentary and photonic coloration mechanisms reveal taxonomic relationships of the Cattlehearts (Lepidoptera: Papilionidae: Parides). *Bmc Evolutionary Biology* 14, 160.

Yoda, S., Sakakura, K., Kitamura, T., KonDo, Y., Sato, K., Ohnuki, R., Someya, I., Komata, S., Kojima, T., Yoshioka, S. et al. (2021). Genetic switch in UV response of mimicry-related pale-yellow colors in Batesian mimic butterfly, Papilio polytes. *Sci Adv* 7.

Zhang, L., Martin, A., Perry, M. W., van der Burg, K. R., Matsuoka, Y., Monteiro, A. and Reed, R. D. (2017a). Genetic Basis of Melanin Pigmentation in Butterfly Wings. *Genetics*.

Zhang, L., Mazo-Vargas, A. and Reed, R. D. (2017b). Single master regulatory gene coordinates the evolution and development of butterfly color and iridescence. *Proc Natl Acad Sci U S A* 114, 10707-10712.

623 **Figure 1.** Hierarchical nanostructure of wing scales in *Parides eurimedes*
624 (Papilionidae). (A) Adult male with structurally-colored green patches on their dorsal
625 forewings. Credit: iDigBio YPM Ent 433579. (B) SEM top-view and (C) FIB-SEM cross-
626 sectional image of an adult green scale showing ridges and honeycomb lattice ending
627 in trabeculae on top of a perforated multilayer lattice. Scale bars: (A) – 1cm, (B and C)
628 – 1μm.
629
630 **Figure 2.** Morphogenetic time series of the development of cuticular disks in pupal *P.*
631 *eurimedes* dorsal forewing scales, acquired with a 100x confocal microscope. AF-555
632 WGA (green) stains chitin and Cellmask (red) stains plasma membrane. By 52%
633 development, Hollow vein-like crossribs appear on plasma membrane in between
634 ridges that serve as a scaffold for cuticle accretion. As scales mature, more cuticle is
635 deposited into these rows of disks bounded by plasma membrane. See also Figs. S4-
636 S6. (B-B''') Close up views of A-A'''. (C-C''') *xz* cross-sections of the scale at locations
637 marked with grey lines in A-A''' reveal the planar aspect of the cuticular disks. Yellow
638 ROI in C'-C''' correspond to those in B'-B'''. Scale bars (A-A''') – 5μm, (B-B''' and C-C''')
639 – 2μm.
640
641 **Figure 3.** Morphogenetic time series of the development of columnar honeycomb
642 lattice in pupal *P. eurimedes* dorsal forewing scale cells acquired with super-resolution
643 lattice SIM. AF-555 WGA (green) stains chitin and AF-647 phalloidin (red) stains F-
644 actin. AF-555 WGA show a gradual evolution of the cuticular disks from filled-in planar
645 to hollow tubular outgrowths. The disintegrating F-actin bundles show evidence of
646 reorganization from linear to reticulated features with ring-like cross-sections. See also
647 Figs. S7-S9. (B-B'') Close up views of A-A''. Insets correspond to the regions of interest

648 (ROI) marked in yellow shown with a 3D aspect. (C-C") *xz* cross-sections of the scale
649 at locations marked with grey lines in A-A". Scale bars (A-A") – 5μm, (B-B", C-C" and
650 insets) – 1μm.
651
652 **Figure 4.** Arp2/3 complex is involved in F-actin reorganization in pupal *P. eurimedes*
653 wing scales. Dorsal forewing scales stained with AF-594 anti-Arp2 (green) and AF-
654 647 phalloidin (red) acquired with 100x confocal microscope. Initially (~52%
655 development), Arp2/3 complex appear as sparse punctate dots while the F-actin
656 bundles are still intact. As F-actin bundles disintegrate and reorganize, a relatively
657 higher density of punctate Arp2/3 signal is seen in close association with the reticulate
658 F-actin network. Our oldest timepoint in *P. eurimedes* (~76% development) has a large
659 amount of cuticle autofluorescence overlapping with the AF594 signal, but the
660 punctate pattern can be still discerned. See also Figs. S10-S12. (B-B") Close up views
661 of A-A". (C-C") *xz* cross-sections of the scale at locations marked with grey lines in A-
662 A". Yellow ROIs correspond to those in B-B". Scale bars (A-A") – 5μm, (B-B" and C-
663 C") – 2μm.
664
665 **Figure 5.** Conservation of honeycomb lattice development in genus Parides. SEM
666 cross-section view of (A) adult green scales in *P. arcas,* (D) blue scales in *P.nireus,*
667 and (G) green scales in *P.palinurus.* All pupal dorsal forewing scales are stained either
668 with AF-555 WGA or FITC-WGA (green) showing chitin, and AF-647 phalloidin or
669 TRITC-phalloidin (red) showing F-actin. (B-C) Maximum projected 3D-SIM micrograph
670 of green cover scales in pupal male *P. arcas* featuring planar cuticular disks similar in
671 shape and arrangement to *P. eurimedes*. (B'-C') Maximum projected 3D-SIM
672 micrograph of green cover scales of a different male *P. arcas* pupa showing irregular

673 crossribs patterns. (E-F) Maximum projected 3D-SIM micrograph of blue cover scales
674 of pupal *P. nireus*, similarly with crossribs and intact linear actin bundles. (H-I) 60x
675 confocal micrographs of green cover scales of pupal *P. palinurus* shown at two
676 different z-planes. A concave network of F-actin underlie the cuticular dimples. At
677 lower *z*, the actin rings (in cross-section) are smaller in size and show a foam-like
678 appearance. (C-C', F, and I) *xz* cross-sections of the scales with ROI at locations
679 marked with grey lines in B-B', E, and H respectively. Scale bars (A, D, and G) – 5μm,
680 (B-B', C-C', E, and F) – 1μm, (H-I) – 5μm.
681
682 **Figure 6**. A schematic illustrating the proposed morphogenesis of honeycomb lattices
683 in papilionid wing scales. During early stages, F-actin bundles prefigure the loci where
684 ridges form in between adjacent actin bundles. Next the plasma membrane (black
685 lines) forms a scaffold where cuticle (green lines and structures) accumulates into the
686 spaces and forms irregular disk-like structures. Reorganization of F-actin around the
687 disks subsequently extrudes the plasma membrane along with the deposited cuticle,
688 forming the honeycomb lattice walls.

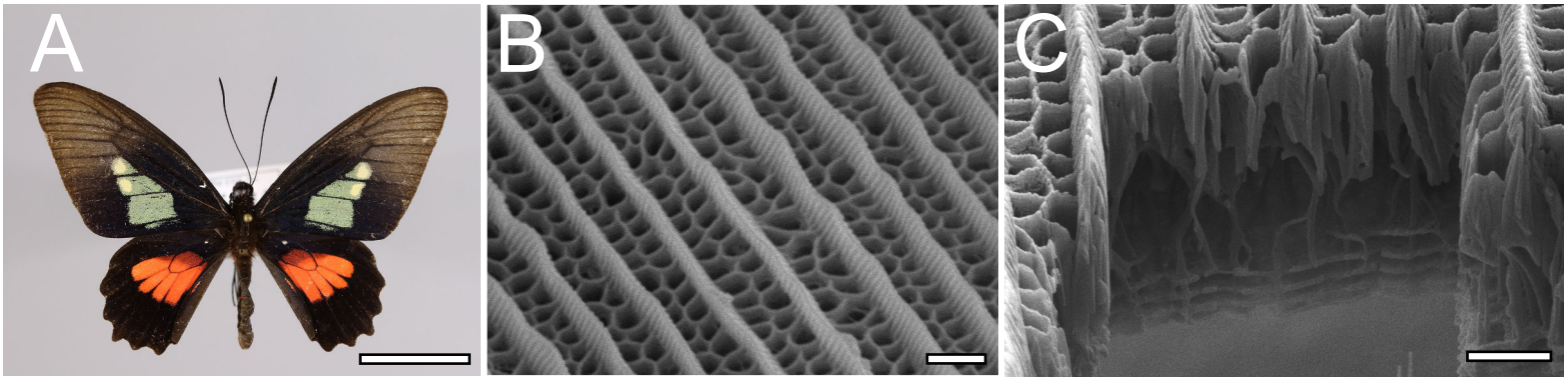
A
B
C

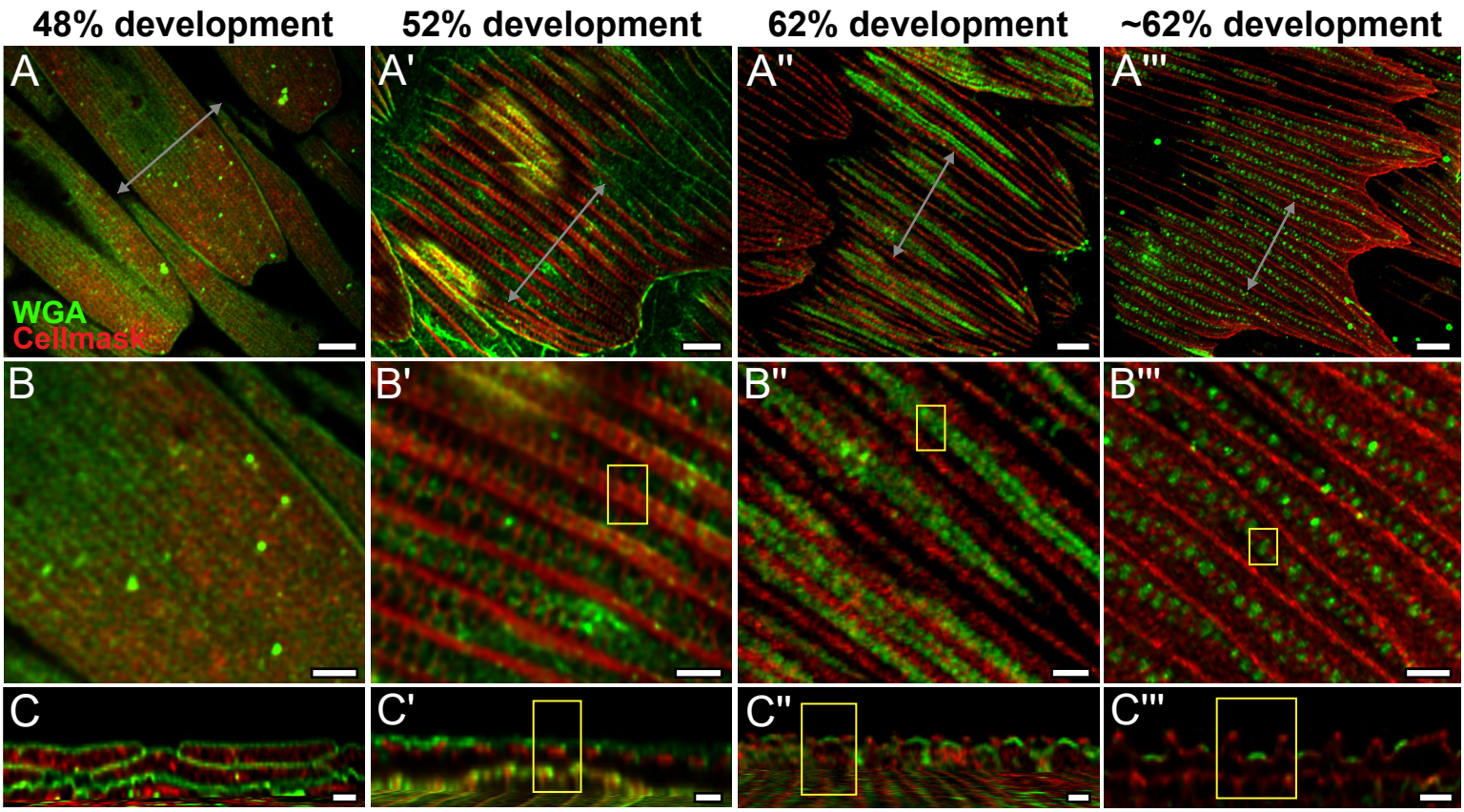
48% development
52% development
62% development
~62% development
A
A'
A''
A'''
WGA
Cellmask
B
B'
B''
B'''
C
C'
C''
C'''

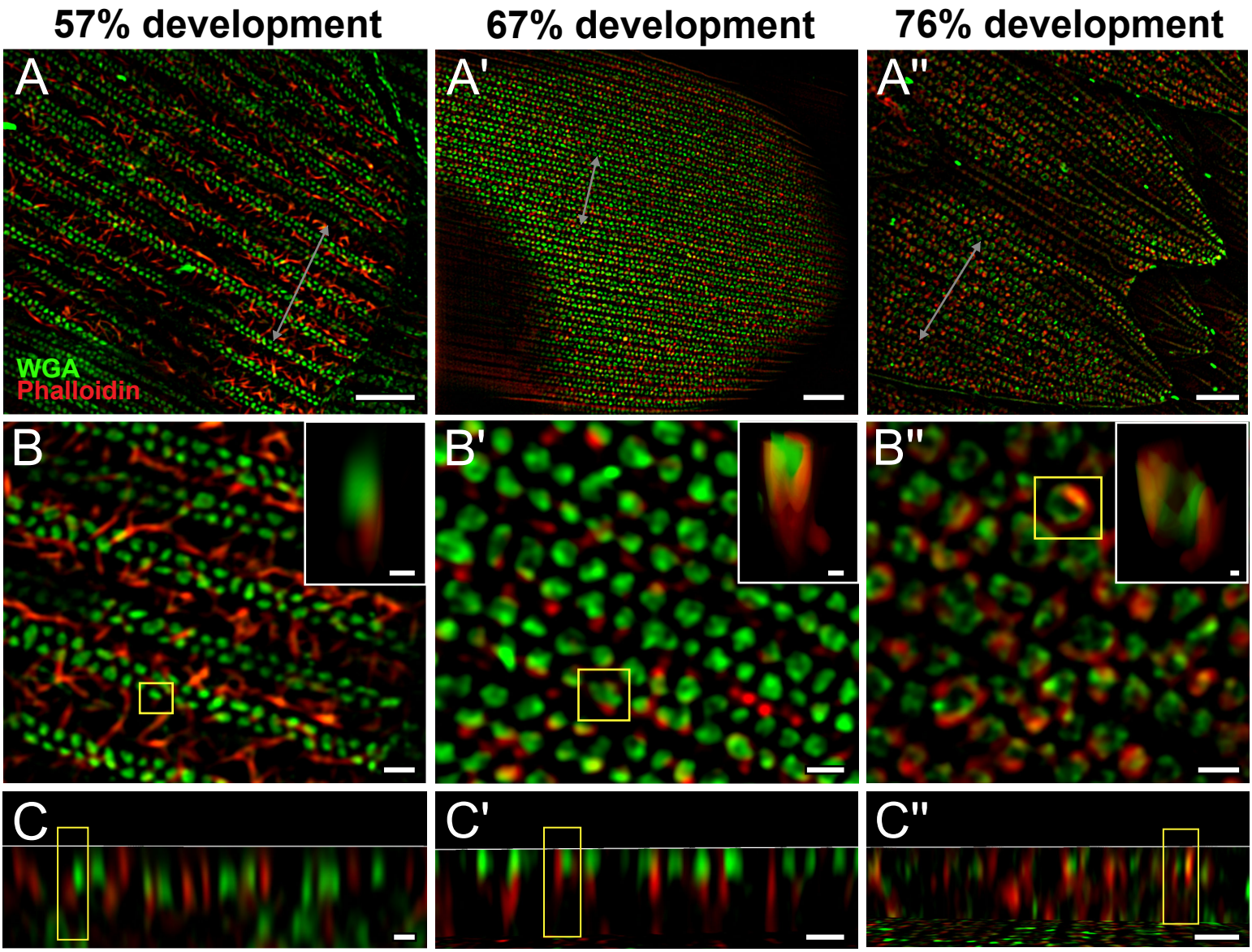
57% development
67% development
76% development
A
A'
A''
WGA
Phalloidin
B
B'
B''
C
C'
C''

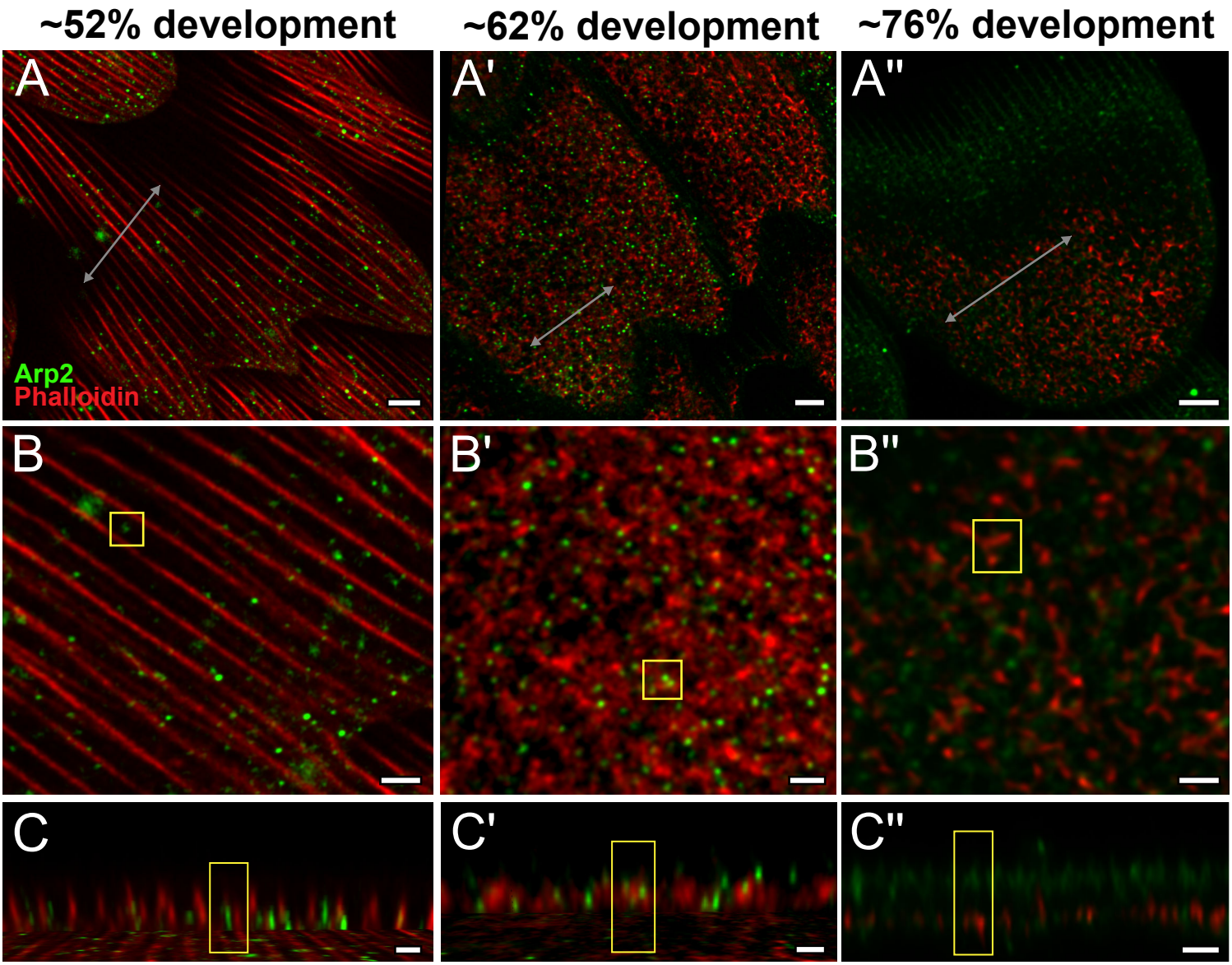
~52% development
~62% development
~76% development
A
A'
A''
Arp2
Phalloidin
B
B'
B''
C
C'
C''

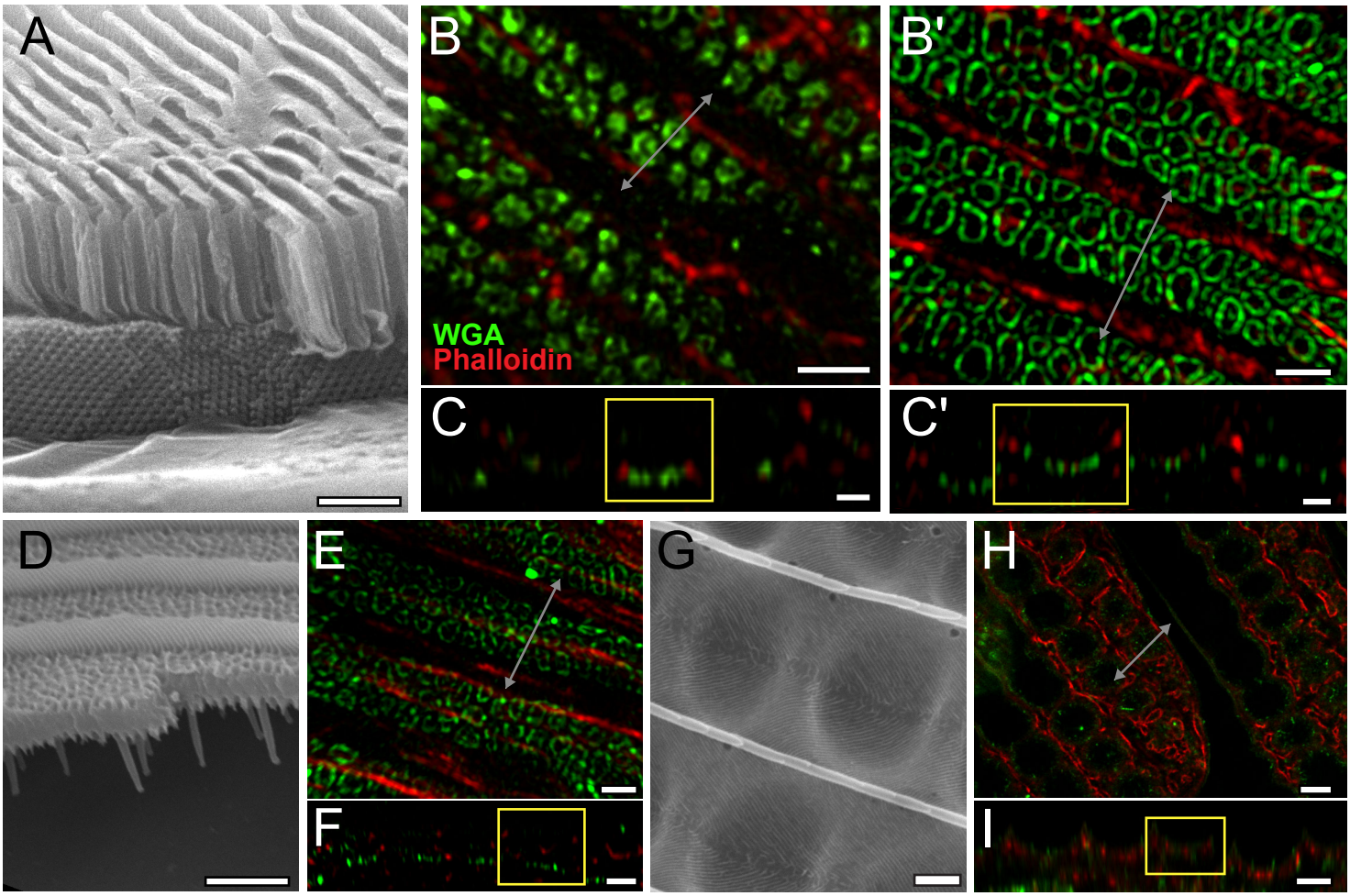
A
B
WGA
Phalloidin
B'
C
C'
D
E
F
G
H
I

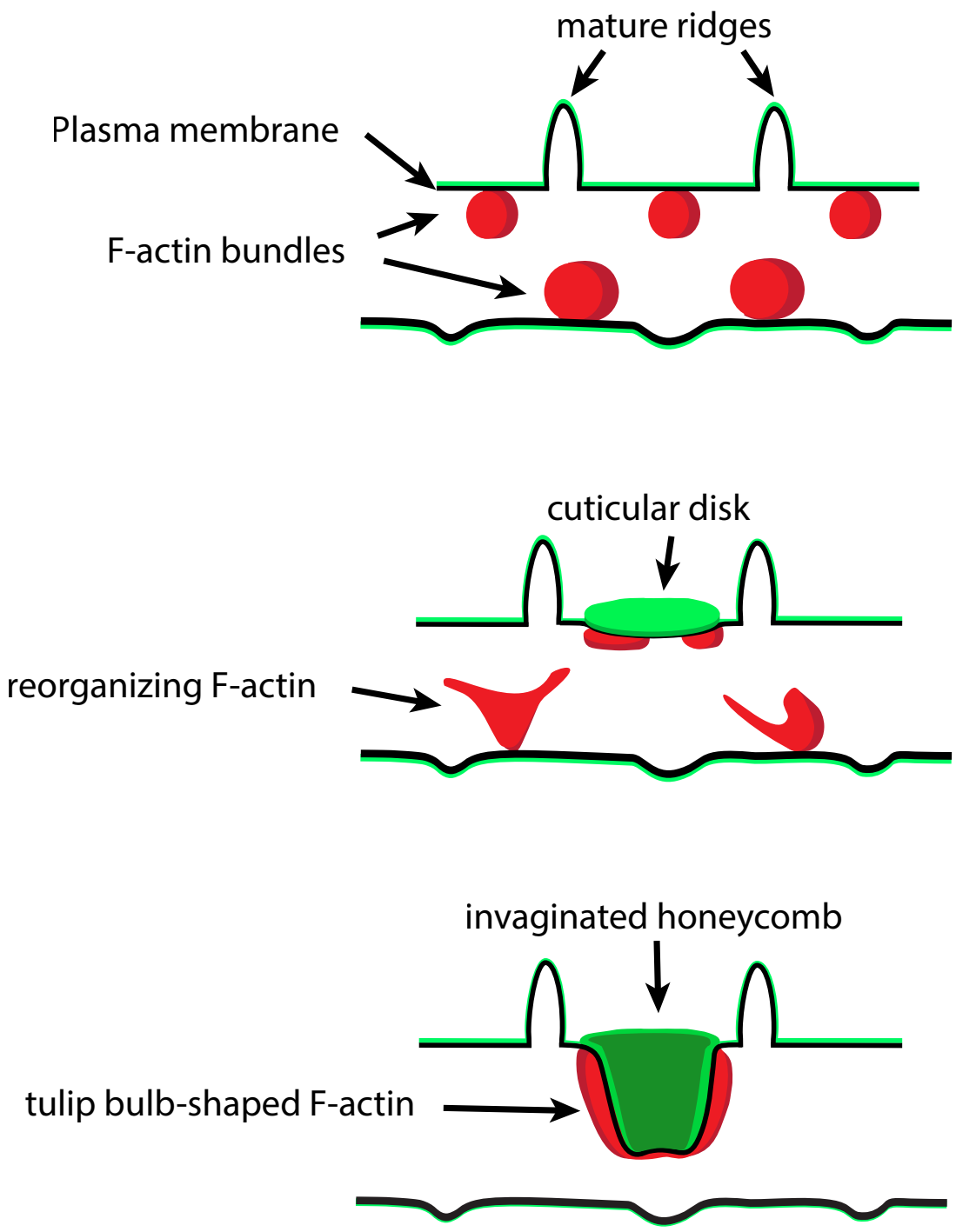
mature ridges
Plasma membrane
F-actin bundles
cuticular disk
reorganizing F-actin
invaginated honeycomb
tulip bulb-shaped F-actin